

AUTOMATED DETECTION OF LUNAR RIDGES BASED ON DEM DATA

M. Peng *, Y. Wang, Z. Yue, K. Di

State Key Laboratory of Remote Sensing Science, Institute of Remote Sensing and Digital Earth, Chinese Academy of Sciences,
Beijing, China - (pengman, wangyx716, yuezy, dikc)@radi.ac.cn

Commission III, ICWG III/II

KEY WORDS: Lunar Wrinkle ridge, DEM, Automatic Detection, Terrain Analysis

ABSTRACT:

Wrinkle ridges are a common feature in the lunar maria and record subsequent contraction of mare infill. Automatic detection of wrinkle ridges is challenging because the ridges are of irregular shapes and many ridges have been eroded and/or degraded over time. The proposed method consists of the following steps. First, as the slope can reflect the gradient changes of the ridge rims to a certain extent, the slope map is generated and converted to a grayscale (0-255) image. Then the phase symmetry of the slope map is calculated with filter wavelength and filter scales parameters, which reduce the regions into symmetry regions. Next, a regional threshold is applied to limit the ridge candidates. Candidates with values less than the threshold are rejected. Moreover, the images are processed using a series of morphological operations, such as close, open, edge linking and noise removal. Finally, after thresholding the ridge map can be obtained. An experiment was performed using Lunar Reconnaissance Orbiter Camera (LROC) WAC image and topographic data from LOLA, the results demonstrate promising performance with detection percentage from 73 to 90.

1. INTRODUCTION

With previous and ongoing Lunar exploration missions, such as the Chinese Chang'E Project, the Japanese Kaguya, the India's Chandrayaan-I and NASA's Lunar Reconnaissance Orbiter (LRO), a vast number of lunar images and topographic data have been acquired. The topographical information in lunar surface consists of craters, rilles, ridges, mountains and grabens. The wrinkle ridge is one of the important geological characteristics on the lunar surface (Barata et al., 2015). Most of the wrinkle ridges are distributed on the lunar maria, and several extend to the vicinity of the highlands (Schultz, 2000). It is usually disconnected, irregular, and may braid or rejoin along strike (Yue et al., 2015). Generally, wrinkle ridges have three major sections: gently sloping on one side, a drop-off in the other side, and a broad platform in the middle.

Researchers have been exploring the important aspects of ridges for a long time. Many researchers have mapped the wrinkle ridges and analyzed their distribution characteristics (e.g., Maxwell et al. 1975; Fagin et al. 1978; Golombek et al. 1991; Walsh et al. 2013). Using a global mosaic of images from the Lunar Reconnaissance Orbiter Camera (LROC) wide-angle camera (WAC), Yue et al. (2015) mapped the population of wrinkle ridges on the Moon. The lunar ridges are categorized into many groups based on their locations and spatial continuity. Furthermore, based on the global ridge map after identifying appropriate boundaries for crater identification, and mapping superposed craters, ridges were analyzed using the buffered crater counting method, the ages of lunar wrinkle ridges are determined (Yue et al., 2017). To determine which kind of factors or processes playing important roles in the formation of the wrinkle ridges in lunar mare basins, the wrinkle ridges are identified manually in Mare Serenitatis and Mare Tranquillitatis, and topographic profiles near its mid-point are made to extract

the maximum height using the LOLA DEM data, finally the $D_{max-L(D-L)}$ ratios are derived by a linear fit method according to the D-L data (Li et al., 2018). Wrinkle ridges in Mare Serenitatis were identified and mapped via high-resolution data acquired from SELENE, and a quantitative method was introduced to analyze the degree of central symmetry of the wrinkle ridges distributed in a concentric or radial pattern (Yao et al., 2018). However, the manual extraction of ridges during these researches is an overly time-consuming and inefficient process.

As ridge is a symmetry feature that is invariant to illumination and contrast, Micheal et al. (2014) proposed a technique based on phase symmetry and phase congruence for automatic ridge detection in lunar images, and the proposed approach provides better results than the plan curvature method. However, for some ridges that are difficult to identify from image, the method is limited. As ridges are of irregular shape and many ridges were eroded and/or degraded over time, it may make the automatic extraction from images infeasible. As wrinkle ridges typically consist of a broad arch and a superposed sharper ridge (e.g., Strom, 1972; Sharp and Head, 1988), this enables them to be distinguished from the surrounding terrains by the slope change (Golombek et al., 1991). Accordingly, designing an automatic ridge detection algorithm based on DEM data is available. In this paper, we proposed a method using phase symmetry and morphological operations.

The rest of this paper is structured as follows: Section 2 summarized the experimental data sets. Section 3 presents and specifies the proposed method; Experimental result is presented in Section 4. Finally, conclusions and suggestions for future work are given in Section 5.

* Corresponding author.

2. DATA

LRO was the first mission in the Lunar Precursor Robotic Program of the National Aeronautics and Space Administration (NASA). LROC had three imaging subsystems, including two narrow-angle cameras (NACs) and one multispectral wide-angle camera (WAC). It was designed to achieve two measurements: obtaining landing site photos with meters scale or smaller scale and determining lunar polar illuminations (Robinson et al., 2010). In this paper, the WAC global mosaic image with a resolution of 100 m/pixel at test sites are used to show the extracted results. This image can be downloaded from the website (http://astrogeology.usgs.gov/search/details/Moon/LRO/LROC_WAC/Lunar_LRO_LROC-WAC_Mosaic_global_100m_June2013/cub).

The Laser Altimeter (LOLA) on board the LRO was used to determine the Digital Elevation Model (DEM) data of the lunar surface with high resolution (Chin et al., 2007). It operated at 28 Hz with a accuracy of 10 cm (Smith et al., 2010). After calibration, the position of each laser spot was determined on the basis of the spacecraft trajectory, altitude history, and a lunar orientation model (Smith et al., 2010). And then the gridded data record products were generated from the laser spots with a resolution of 30 m/pixel at the equator (<http://geo.pds.nasa.gov/missions/lro/lola.htm>). In this study, we chose 6 sub areas to test our method. The distribution of the test sites is shown in Fig. 1. The green dots represent the center locations of the test images. The experimental DEM area are selected from lunar maria, which are the areas in which ridges most likely lie. The reference data used for detection accuracy assessment are collected by manual digitization from WAC images.

3. METHOD

As some ridges are difficult to extract from images for its low contrast, while the slope reflects the gradient changes of the wrinkle ridges to a certain extent, it can be used to extract ridges automatically. The proposed procedure includes slope map generation, phase symmetry processing, morphological operation, and noise removal. First, the slope map is generated and converted to grayscale image for post processing. Then the phase symmetry of the slope map is calculated with filter wavelength and filter scales parameter, which reduced the regions into symmetry regions. Next, a regional threshold is applied to limit the ridge candidates. Candidates with values less than the threshold are rejected. Moreover, the images are processed using a series of morphological operations, such as close, open and edge linking. Finally, after thresholding the significant ridge can be determined.

3.1 Slope map generation

For each pixel, slope represents the maximum rate of change in value from that pixel to its neighbors. Basically, the maximum change in elevation over the distance between the pixel and its eight neighbors identifies the steepest downhill descent from the pixel.

The rates of change of the surface in the horizontal and vertical directions from the center pixel determine the slope. The slope is calculated using

$$S = \arctan \sqrt{p^2 + q^2} \quad (1)$$

While S is the slope value, p is the changing rate of elevation in horizontal direction, q is the changing rate of elevation in vertical direction.

A plane is fit to the height values of a 3 x 3 neighborhood around the processing or center pixel. The slope value of this plane is calculated using the average maximum technique. The lower the slope value, the flatter the terrain; the higher the slope value, the steeper the terrain.

3.2 Phase symmetry processing

Ridge is a symmetry feature in DEM that is invariant to illumination and contrast, symmetry detection method can be used. However, most approaches require objects to be segmented prior to symmetry analysis. Based on the local frequency information measurement proposed by Kovese (1997), ridge can be enhanced from other objects.

According to phase patterns of symmetry and asymmetry points, the absolute value of the even-symmetric filter is large and the absolute value of the odd-symmetric filter is low (Kovese, 1997), thus, symmetry can be measured by determining the absolute value of the even-symmetric filter output. Generally wavelet transform are used for frequency analysis, Log Gabor function can construct large bandwidth filters while maintaining a zero DC component in the even-symmetric filter.

Firstly signal is convolved with each of the quadrature pairs of wavelets, suppose I denote the signal, M_n^e and M_n^o represent the even-symmetric and odd-symmetric wavelets at a scale n , each quadrature pair of filters results can form a vector.

$$[e_n(x), o_n(x)] = [I(x) * M_n^e, I(x) * M_n^o] \quad (2)$$

where $e_n(x)$ and $o_n(x)$ can be seen as real and imaginary parts of complex valued frequency component. The amplitude of the transform at a given wavelet scale is given by

$$A_n(x) = \sqrt{e_n(x)^2 + o_n(x)^2} \quad (3)$$

and the phase is given by

$$\phi_n(x) = a \tan 2(e_n(x), o_n(x)) \quad (4)$$

To combine information from filter responses over multiple scales, a weighted average is formed. It is the difference between the absolute values of an even and odd filter responses at each scale which is weighted by the magnitude of the filter response vector at each scale A_n in Eq. (3). The sum of these weighted differences is

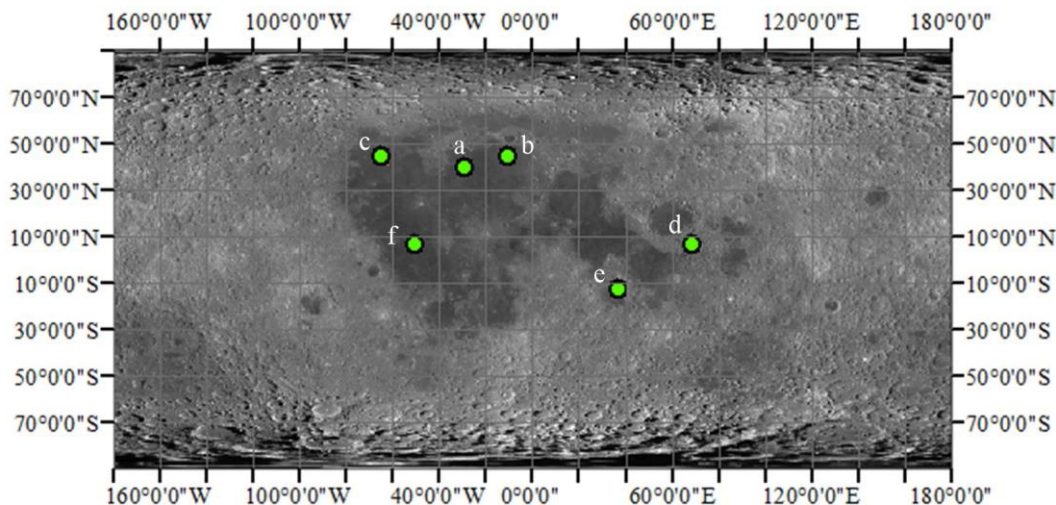


Figure 1. Location map of the six test sites

$$Sym(x) = \frac{\sum_n \lfloor A_n(x) [\cos(\phi_n(x)) - |\sin(\phi_n(x))|] - T \rfloor}{\sum_n A_n(x) + \varepsilon} \quad (5)$$

$$= \frac{\sum_n \lfloor [e_n(x) - |o_n(x)|] - T \rfloor}{\sum_n A_n(x) + \varepsilon}$$

Where $e_n(x)$ is the even symmetric part and $o_n(x)$ is the odd symmetric part of the filter in n scales. The \sum_n joins the information of several filters at different scales. At a point of symmetry the absolute value of $e_n(x)$ will be large and the absolute value of $o_n(x)$ will be small. The term ε is a constant to prevent division by zero in case where the signal is uniform and no filter response is obtained. The factor T is a noise compensation term combining the estimated influence of noise on each of the filters.

3.3 Morphological operation

A lot of pixel noise interferes with the lunar ridge detection; therefore morphological processing is used. The symmetry map are processed using morphological operations for thinning, noise removal. Firstly, the morphological closed operation is performed, which dilates the symmetry map and then erodes it to enhance the edge and eliminate the noise. The regions are expanded with a disk-shaped structure element of radius 3. Then the noise removal algorithm is performed including opening operation and small area elimination. The morphological open operation is used to dilate the object whose area is less than a threshold P , it can exclude the small detected objects and other noises. In practice, P is set to 30. Furthermore, to eliminate square areas (which may be craters), the length ratio is calculated as:

$$r = \frac{d_{\max} - d_{\min}}{d_{\max} + d_{\min}} \quad (6)$$

Where d_{\max} and d_{\min} represent the maximum and minimum distances between the detected region's point and its mass center. As the ridge is linear in our experiments, the detected areas are remained if r is larger than 0.7. Finally, the remaining

objects are linked by adjacent and similar direction properties in order to form the detected regions.

4. EXPERIMENT

We have applied the proposed method to six test sites from LOLA DEM. The image and DEM of test sites used for the experiment are shown in Figs.2 and 3 respectively. As shown in Fig 4, the slope map reveal more ridge details and the background information in Fig 2 are suppressed. Fig 5 shows the results obtained from the phase symmetry measure. Fig 6 shows the automatically detected region (red line) on WAC image, the results are calculated though the geographic coordinates from DEM

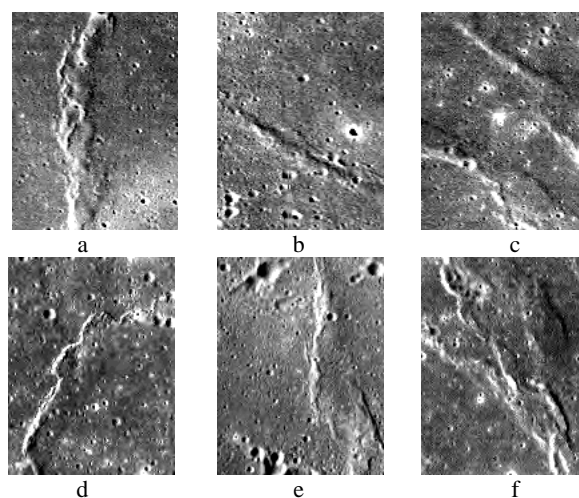
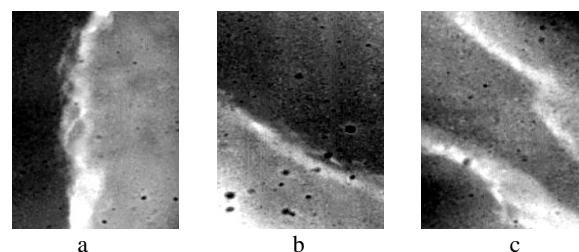


Figure 2. The WAC images of lunar ridges at test sites



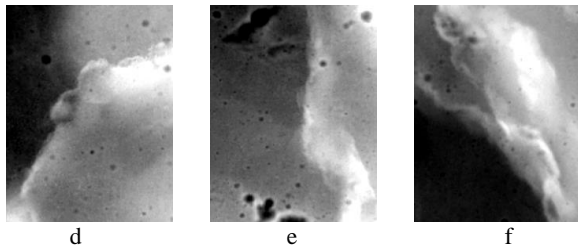


Figure 3. DEM data at test sites

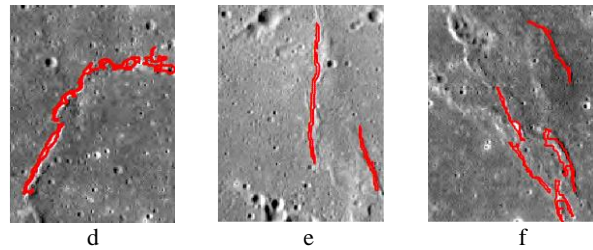


Figure 6. Ridge detection results at test sites

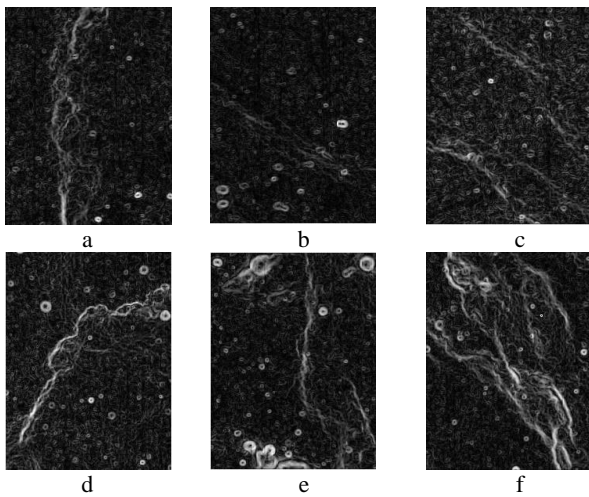


Figure 4. Slope map of lunar ridges at test sites

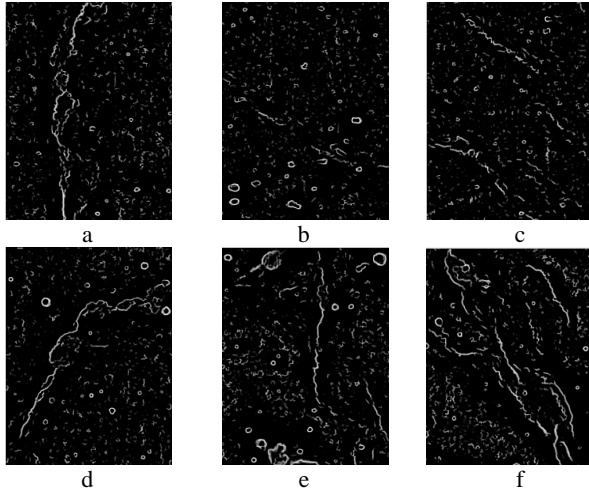
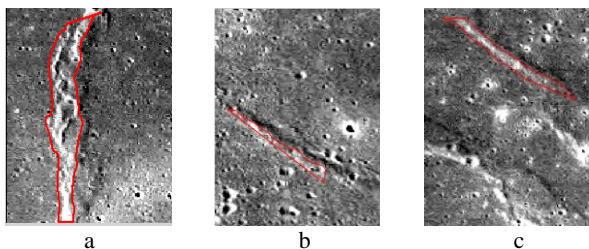


Figure 5. Results obtained from the phase symmetry measure.



Furthermore, manual verification for each test site was performed and acts as ground truth for the quantitative assessment. Detection percentage $D = 100TP / (TP + FN)$ is used to evaluate the performance of our method, where TP stands for the number of true positive detections, FP the number of false positive detections, and FN the number of false negative detections (Swets, 1988). The parameter D can be treated as a measurement of the detection performance (the larger, the better).

The detected ridges are counted and compared with the manually delineated ridges to calculate the quality factors, in which the manually delineated ridges are considered as the reference data. The assessment factors are computed according to the following principles: the detected pixels which are coincided with the manually delineated ones are considered to be a true positive detection (TP); otherwise, it is a false positive detection result (FP); for those manually delineated ridges which are not covered by detection results are counted as false negative detection results (FN). Table 1 lists the performance quality factors of the six test sites.

Table 1. Ridge detection quality factors

Test sites	TP	FP	FN	D
a	0.907	0.018	0.093	90.7%
b	0.739	0	0.251	73.9%
c	0.822	0	0.178	82.2%
d	0.840	0.006	0.160	84%
e	0.772	0.002	0.228	77%
f	0.730	0.001	0.270	73%

From Table 1, the detection percentage is always higher than 73 percent, indicating most ridges can be correctly detected by this method. Site *a* has the highest detection percentage because the ridges cover larger areas. Site *f* has the lowest detection percentage, because there exists multiple ridges in this area. The detection performance is affected by the morphology of the ridge and the complexity of the background. The eroded ridges with inconspicuous difference from the background are usually undetected. Other small features with similar morphology to ridges tend to increase false detection. Some wide ridges are also undetected because small size parameter is set for the structuring element in close transformation to reduce false positive detection.

It's a preliminary study of automated ridge detection from DEM data. In the six test sites, most of the ridges are correctly detected and the false positive detection is restrained at a low level. In principle, the method may be also applied to other linear target detection.

5. CONCLUSION

This paper presents an automated method for lunar wrinkle ridges detection from DEM data based on phase symmetry

processing and mathematical morphology techniques. The method also integrates a series of morphological operators, including area opening and closing. Experimental results at six sites show that the proposed automated method achieves good performance with accuracy values ranging between 73 percent and 90 percent. In the future, the method will be further improved to enhance its robustness and applicability by integrating other techniques such as machine learning. DEM data will be better used to calculate the geoscience attributions of the ridges such as SOA(slope of aspect) and direction.

ACKNOWLEDGEMENTS

This study was supported by the Key Research Program of the Chinese Academy of Sciences, Grant NO.XDPB11 and National Natural Science Foundation of China under Grants 41771488 and 41701489.

REFERENCES

- Barata MT, Lopes FC, Pina P, Alves EI, Saraiva, 2015. Automatic detection of wrinkle ridges in venusian magellan imagery. *Geol Soc Lond Spec Publ* 401:357–376
- Chin, G., Brylow, S., Foote, M., Garvin, J., Kasper, J., Keller, J., ... and Robinson, M., 2007. Lunar reconnaissance orbiter overview: The instrument suite and mission. *Space Science Reviews*, 129(4), 391-419.
- Fagin, S. W., D. M. Worrall, and W. R. Muehlberger, 1978, Lunar mare ridge orientations: Implications for lunar tectonic models, *Proc. Lunar Planet. Sci. Conf.*, 9, 3473–3479.
- Golombek, M. P., J. B. Plescia, and B. J. Franklin, 1991, Faulting and folding in the formation of wrinkle ridges, *Proc. Lunar Planet. Sci. Conf.*, 21, 679–693.
- Maxwell T A, El-Baz F, Ward S H. Distribution, morphology, and origin of ridges and arches in Mare Serenitatis, 1975. *Geological Society of America Bulletin*, 86(9): 1273-1278.
- Kovesi, P., 1997. Symmetry and asymmetry from local phase. In: *Proceedings of the Tenth Australian Joint Conference on Artificial Intelligence*, Perth, 185–190.
- Li, B., Ling, Z., Zhang, J., Chen, J., Ni, Y., and Liu, C., 2018. Displacement-length ratios and contractional strains of lunar wrinkle ridges in Mare Serenitatis and Mare Tranquillitatis. *Journal of Structural Geology*, 109, 27-37.
- Micheal A A, Vani K, Sanjeevi S. Automatic detection of ridges in lunar images using phase symmetry and phase congruency, 2014. *Computers & geosciences*, 73: 122-131.
- Robinson, M. S., Brylow, S. M., Tschimmel, M., Humm, D., Lawrence, S. J., Thomas, P. C., ... and Caplinger, M. A. ,2010. Lunar reconnaissance orbiter camera (LROC) instrument overview. *Space science reviews*, 150(1-4), 81-124.
- Schultz RA, 2000. Localization of bedding plane slip and backthrust faults above blind thrust faults: keys to wrinkle ridge structure. *J Geophys Res* 105(E5):12035–12052
- Sharpton, V. L., and J. W. Head, 1988. Lunar mare ridges: Analysis of ridge-crater intersections and implications for the tectonic origin of mare ridges, *Proc. Lunar Planet. Sci. Conf.*, 18, 307–317.
- Smith, D. E., Zuber, M. T., Jackson, G. B., Cavanaugh, J. F., Neumann, G. A., Riris, H., ... and Katz, R. B., 2010. The lunar orbiter laser altimeter investigation on the lunar reconnaissance orbiter mission. *Space science reviews*, 150(1-4), 209-241.
- Strom, R. G., 1972, Lunar mare ridges, rings and volcanic ring complexes, *Mod. Geol.*, 2(2), 133–157, doi:10.1007/978-94-010-2861-5_19.
- Swets, J., 1988. Measuring the accuracy of diagnostic systems, *Science*, 240(4857):1285 - 1293.
- Walsh, L. S., T. R. Watters, M. E. Banks, and S. C. Solomon , 2013. Wrinkle ridges on Mercury and the Moon: A morphometric comparison of length–relief relations with implications for tectonic evolution, *Lunar Planet. Sci.* 44. Abstract #2937.
- Yao, M., and Chen, J. ,2018. The Central Symmetry Analysis of Wrinkle Ridges in Lunar Mare Serenitatis. *Earth, Moon, and Planets*, 121(1-2), 45-58.
- Yue, Z., Li, W., Di, K., Liu, Z., Liu, J., 2015. Global mapping and analysis of lunar wrinkle ridges. *J. Geophys. Res., Planets* 120 (5), 978–994.
- Yue, Z., Michael, G. G., Di, K., and Liu, J., 2017. Global survey of lunar wrinkle ridge formation times. *Earth and Planetary Science Letters*, 477, 14-20.